ChemCatChem

Research Article
doi.org/10.1002/cctc.202401947

Chemistry Europe
European Chemical Societies Publishing

www.chemcatchem.org

# Selective Light-Driven $CO_2$ to CO Reduction by a [FeFe]-Hydrogenase Mimic in Water

Amir Abbas,[a] Chizuru Kasahara,[b, c] Yongchao Chen,[d] Martin Oschatz,[d, e, f] Stefanie Gräfe,[c, e, g, h] Wolfgang Weigand,[b] and Andrea Pannwitz*[a, b, e, f, g, h]

We report a biomimetic system for light-driven $CO_2$ conversion in lipid bilayers using a [FeFe]-hydrogenase-inspired molecular dyad (**PS-CAT**) acting simultaneously as photosensitizer and catalyst. The molecular design of **PS-CAT** consists of both light-harvesting and catalytically active moieties in a single molecule. This structure allows for efficient charge transfer between these two moieties. The **PS-CAT** consists of only an organic chromophore and an iron complex. Photocatalytic reduction of $CO_2$ to CO ($CO_2$RR) as well as $H_2$ production (HER) was traced over 56 h to determine $CO_2$RR/HER selectivity. The presence of water in the lipid bilayer system allows for $CO_2$RR selectivity >99 % over the competitive HER, outperforming previous molecular, and liposome-based systems for light-driven $CO_2$ to CO conversion. The product selectivity in $CO_2$RR (e.g., CO, $HCOO^-$, and $CH_4$) was determined via gas chromatography and NMR spectroscopy with $^{13}$C-labeled carbon sources. The Stern–Volmer quenching studies on the initial light-driven electron-transfer revealed static quenching and indicated a preassembly of the **PS-CAT** with the electron donor at the membrane-water interface.

## 1. Introduction

In nature, light-driven $CO_2$ conversion takes place in cellular compartments, known as chloroplasts (Figure 1A). The actual light-harvesting and initial light-energy conversion occurs within the phospholipid bilayer, which assembles the reactive molecular components and proteins with a predominant function of spatial arrangement.[1,2] In artificial systems, the assembly in lipid bilayers can facilitate electron transfer dynamics between the active units,[3,4] can protect the active unit toward decomposition,[3,5,6] and enables to conduct reactions in water despite the hydrophobic character of the PS and CAT.[4,7,8] Light energy conversion in artificial photocatalytic and bioinspired systems typically consists of three components (Figure 1B): a photosensitizer (PS), a catalyst (CAT), and a sacrificial electron donor (SED). However, most of these studies do not use a biomimetic assembly strategy such as lipid bilayers.[9–11] Usually, the PS and CAT are based on second and third row transition metals (e.g., Ru, Pt, and Cd) because of their stability and (photo-)redox chemistry, at the cost of low abundance, high prices, or undesirable side effects such as toxicity.[12–17] It is therefore desirable to replace PS and CAT with organics or earth-abundant metal-based complexes. Considering light-driven $CO_2$ reduction, the most pressing limitation is reaction selectivity (i.e., $H_2$ production vs. $CO_2$ reduction) as well as the limitation of charge transfer between PS and CAT.[18] Additionally, most light-driven $CO_2$ reduction case studies are limited to organic solvents to ensure sufficient solubility and to suppress competing $H_2$ generation.[19–21] Therefore, earth-abundant metal complex for light-driven $CO_2$RRs in aqueous conditions are of interest for more sustainable $CO_2$RR.

Herein, we report on a **PS-CAT** dyad that combines an organic PS with an iron-based CAT in one molecule, assembled

[a] A. Abbas, A. Pannwitz
Institute of Inorganic Chemistry I, Ulm University, Albert-Einstein-Allee 11 89081, Ulm, Germany
E-mail: andrea.pannwitz@uni-jena.de

[b] C. Kasahara, W. Weigand, A. Pannwitz
Institute for Inorganic and Analytical Chemistry, Friedrich Schiller University Jena, Humboldtstraße 8 07743, Jena, Germany

[c] C. Kasahara, S. Gräfe
Institute of Physical Chemistry, Friedrich Schiller University Jena, Lessingstraße 4 07743, Jena, Germany

[d] Y. Chen, M. Oschatz
Institute for Technical and Environmental Chemistry, Friedrich Schiller University Jena, Philosophenweg 7a 07743, Jena, Germany

[e] M. Oschatz, S. Gräfe, A. Pannwitz
Center for Energy and Environmental Chemistry Jena (CEEC Jena), Friedrich Schiller University Jena, Philosophenweg 7a 07743, Jena, Germany

[f] M. Oschatz, A. Pannwitz
Helmholtz Institute for Polymers in Energy Applications Jena (HIPOLE Jena), Lessingstraße 12–14 07743, Jena, Germany

[g] S. Gräfe, A. Pannwitz
Abbe Center of Photonics, Friedrich Schiller University Jena, Albert-Einstein-Straße 6 07745, Jena, Germany

[h] S. Gräfe, A. Pannwitz
Fraunhofer Institute of Applied Optics and Precision Engineering, Albert-Einstein-Str. 7 07745, Jena, Germany

Amir Abbas and Chizuru Kasahara contributed equally to this work.

Supporting information for this article is available on the WWW under https://doi.org/10.1002/cctc.202401947

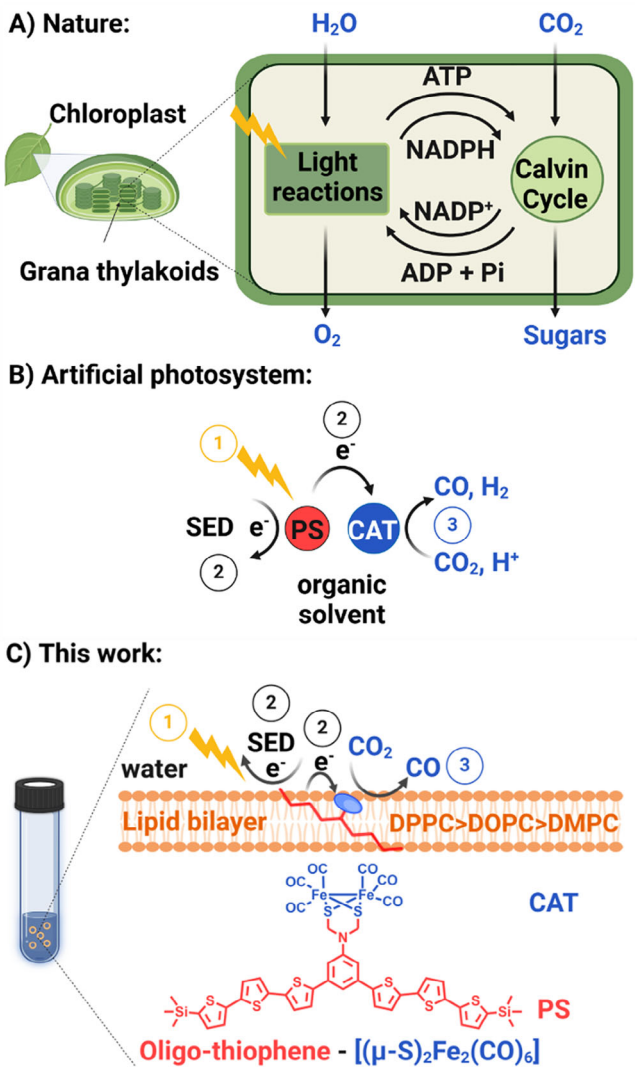


**Figure 1.** Light-driven $CO_2$ reduction, depicting the electron-transfer steps and reaction pathways in: (A) Natural photosystem within the thylakoid membrane in chloroplasts. (B) Artificial photocatalytic system in an organic solvent consisting of three components: photosensitizer (PS), catalyst (CAT), and sacrificial electron donor (SED). (C) Our bioinspired system, employing liposomes as membrane for assembling molecular dyad photocatalyst (PS-CAT), together with sodium ascorbate as sacrificial electron donor (SED). Created with Biorender.com.

within a biomimetic lipid bilayer of liposome vesicles in water. This architecture features high selectivity and activity in visible light-driven $CO_2$ to CO reduction over competitive $H_2$ production (Figure 1C). The organic PS moiety consists of an oligo-thiophene covalently linked to a [FeFe]-hydrogenase mimic (CAT) as a $CO_2$ reduction catalyst. Although there are many reports on (light-driven) $H_2$ evolution by [FeFe]-hydrogenase mimics,[22–24] light-driven $CO_2$ reduction by the [FeFe]-hydrogenase mimics is scarcely known, and in particular the selectivity of $CO_2$ to CO reduction is usually less than unity.[25–29] Our combination of PS and CAT within the same molecule is beneficial for electron transfer (ET) between PS and CAT. This is a very important aspect considering the complexity of the overall process, involving the coordination of $CO_2$ and $H^+$ to the reaction center, the two electron transfer steps, and multiple bond rearrangements over the photocatalytic process.[30,31] The use of lipid vesicles ensures dispersibility in pure buffered water as well as mild reaction conditions.[5,7,8,10,32,33]

By changing the solvent to water, we report here on a qualitative and quantitative change in the selectivity of a [FeFe]-hydrogenase mimic to $CO_2$ reduction instead of $H_2$ evolution under very mild ambient conditions and slightly acidic pH (pH 6.9) in water.

## 2. Results and Discussion

### 2.1. Synthesis and Structural Characterizations of Liposomes

Initially, three types of liposomes comprising **PS-CAT** as the catalyst were prepared, using different phospholipids (see Supporting Information for details on sample preparation). DPPC (1,2-dipalmitoyl-sn-glycero-3-phosphocholine; 16:0 PC, gel phase at room temperature), DOPC (1,2-dioleoyl-sn-glycero-3-phosphocholine; 18:1 (Δ9-Cis) PC, fluid phase at room temperature), and DMPC (1,2-dimyristoyl-sn-glycero-3-phosphocholine; 14:0 PC, fluid and gel phase at room temperature) were selected as the main phospholipids (Table S1). In typical liposomes, **PS-CAT** was incorporated within the phospholipid bilayer in a 100:1:0.5 molar ratio of the (main lipid):(14:0 PEG2000 PE):**PS-CAT**. The lipid bilayer structure of the liposomes was formulated by the thin film hydration method (Figure S1) in sodium hydrogencarbonate solution (0.1 M), as described in previous studies.[3]

Subsequently, the size distribution of the light-active liposomes was characterized by dynamic light scattering (DLS). The hydrodynamic diameter ($Z_{Avg}$) of each liposome was in the range of 130–170 nm before irradiation and 103–176 nm after irradiation (Figure S2 and Table S2) which was in line with similar systems previously studied.[3] Moreover, the **PS-CAT** spectroscopic behavior was studied in DPPC-based liposome membrane and organic solvent respectively, by UV–vis and emission measurements. The characteristic absorption band at $\lambda_{Abs} = 397$ nm and three emissions bands at $\lambda_{Emi} = 455$, 487, and 520 nm of **PS-CAT** were detected in all cases (Figure 2A). In the DPPC-based sample, a broadening and slight red shift of the absorption band ($\lambda = 405$ nm) were observed, that might be caused by interaction with the lipid membrane[34] (Figure 2A). Furthermore, confocal microscopy imaging of **PS-CAT**-loaded giant DPPC liposomes proved the presence and illustrated the distribution of **PS-CAT** in the lipid bilayer. The multilamellar vesicle structure was observed, and fluorescence imaging revealed the presence of emissive compounds, that is molecular dyads, located within the phospholipid bilayer (Figure 2B). Additionally, the strong fluorescence intensity at the liposome boundaries highlights the relatively high aggregation of **PS-CAT** at the membrane-water interface (Figure 2B).

### 2.2. Light-Driven $CO_2$ Reduction

Visible light-driven $CO_2$ reduction reactions ($CO_2$RRs) by **PS-CAT** were performed in buffered water with the **PS-CAT** loaded lipo-

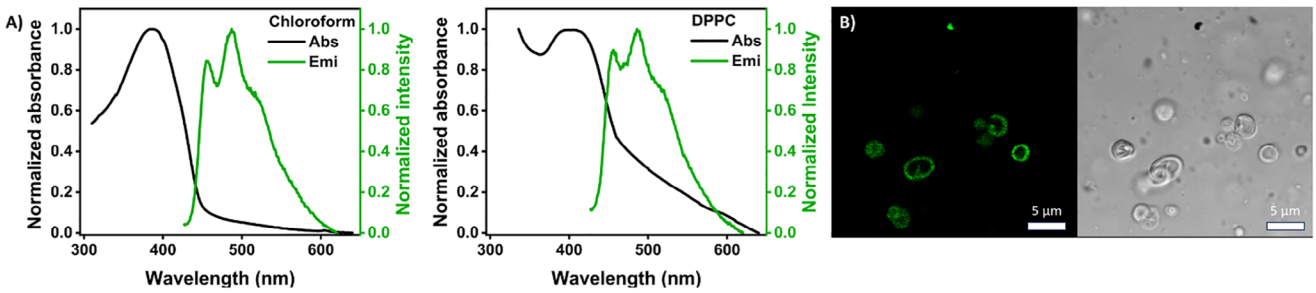


**Figure 2.** (A) UV–vis and emission spectra of PS-CAT (2.3 µM) in chloroform as an organic solvent and in DPPC/water. (B) Confocal microscopy images of giant DPPC vesicles in 100:1:0.5 molar ratio of (main lipid):(14:0 PEG2000 PE):PS-CAT, with c(main lipid) = 5 mM; upon fixation in an agarose hydrogel.

somes. Sodium ascorbate (0.1 M) was selected as the SED, and $CO_2$ atmosphere and saturation were ensured by bubbling $CO_2$ through a constant flow (see Supporting Information) prior to the reaction, reaching an average pH of 6.9 in all cases. All photocatalytic $CO_2$RR samples were irradiated at 405 nm in an open-source and modular 3D-printed photoreactor (Figure S3).[35] Catalytic performance was evaluated in terms of the turnover numbers (TON), turnover frequencies (TOF), and the reaction selectivity of $CO_2$RR. The TON, TOF, and selectivity between $CO_2$RR and HER were calculated by following the Equations (1–3), respectively. It shall be noted that the targeted $c_{PS\text{-}CAT}$ was constant in all samples (1.5 µM), and the phospholipid concentration was 300 µM in all cases unless otherwise described. For the conversion from the concentration to the amount of substances (see Supporting Information on page 6). The TONs were calculated using the target **PS-CAT** concentrations, assuming that all added catalyst was taken up within the membrane during sample preparation.

$$TON_{CO} = \frac{n\,(CO)}{n\,(PS-CAT)} \quad (1)$$

$$TOF_{CO}\left(h^{-1}\right) = \frac{dTON}{dt} \quad (2)$$

$$\text{Selectivity of CO (\%)} = \frac{n\,(CO)}{n\,(H_2)+n\,(CO)} \cdot 100 \quad (3)$$

Photocatalytic $CO_2$RR of **PS-CAT** in DPPC-based liposomes ($DPPC_{PS\text{-}CAT}$) in the presence of $CO_2$ and the sacrificial electron donor sodium ascorbate produced CO with a $TON_{CO} = 331 \pm 38$, over 56 h of irradiation (Table 1). The more noteworthy discovery was that $DPPC_{PS\text{-}CAT}$ exhibited a CO selectivity >99 % (Table 1) according to gas chromatography of the gas phase with a detection limit of 0.05 nmol $L^{-1}$. In some reactions, non-reproducible, small amounts of $H_2$ were detected as a byproduct during the first hours of the $CO_2$RR experiments but vanished over the course of the long reaction time (Figures S4 and S5). Consequently, the $CO_2$RR selectivity against the competitive HER was concluded to be >99 %. Subsequently, the product selectivity in $CO_2$RR (e.g., CO, $HCOO^-$, and $CH_4$) was investigated by the combination of GC and NMR spectroscopy. The absence of $CH_4$ was confirmed by GC-BID (Figures S4 and S5), and no $C_2$ products such as $C_2H_4$ or $C_2H_6$, were detected by a GC-FID (flame ionization detector, Figures S9 and S10). Consequently, the gas product from $CO_2$RR was concluded to be >99 % of CO selectivity. For the liquid phase products, traces of formate were detected by $^1$H NMR spectroscopy, but no corresponding signal could be detected by $^{13}C\{^1H\}$ NMR when using $^{13}C$ isotope labeled carbon sources of $^{13}CO_2$ and $NaH^{13}CO_3$ (Figures S16 and S17). We therefore deduce that the detected formate traces originate from the decomposition of lipid, ascorbate electron donor or **PS-CAT** and not from $CO_2$ reduction. Hence, we concluded on >99% selectivity for light-driven $CO_2$ to CO conversion against $H_2$ production and other $CO_2$ reduction products, which is quantitative and unprecedented among molecular systems in self-assembled lipid bilayers,[2,11,33,36] and superior or very similar to recent molecular systems with iron-based catalysts.[26,27,37,38]

Control experiments with irradiation of $DPPC_{PS\text{-}CAT}$ in the absence of $CO_2$ with ascorbate present yielded $TON_{CO} = 11 \pm 2$, while in both the absence of $CO_2$ and ascorbate yielded $TON_{CO} = 6 \pm 2$. The observed CO was due to ligand dissociation ($TON_{CO} = 6$ = number of CO ligands)[24] and small amounts of $CO_2$ from ascorbate decomposition[39] under photoirradiation ($TON_{CO} = 11$). Furthermore, photocatalytic $CO_2$RRs were performed in homogeneous organic solutions to clarify the effect of the role of water and phospholipids (Table 1, entries 12 and 13). In N-methyl-2-pyrrolidone (NMP) with 1,3-dimethyl-2-phenylbenzimidazoline (BIH) as a sacrificial electron donor, similar to $H_2$ evolution conditions,[30,31] the $TON_{CO}$ was 17 which was significantly lower than in $DPPC_{PS\text{-}CAT}$ liposomes in water. Additionally, the selectivity for CO was relatively low due to $H_2$ formation ($TONH_2 = 5$ and selectivity of CO = 76%, after 24 h, Figure S7). On the contrary, the addition of water to the NMP-solvent resulted in the selectivity of CO > 99% with $TON_{CO} = 35 \pm 5$ (Figure S8), evidently, the presence of water yielded high selectivity. Consequently, pure aqueous solvent condition, which is achieved by a lipid bilayer, enables high CO selectivity and TONs.

To elucidate the effect of the local environment due to the different hydrocarbon chains of the phospholipids,[1,7,40,41] photocatalytic $CO_2$RRs were also carried out for DOPC- and DMPC-based liposomes. DOPC and DMPC have a zwitterionic head group. Under experimental conditions at room temperature, DOPC is in the fluid phase and DMPC is at the transition temperature ($T_m$), whereas DPPC is in the gel phase. The results revealed that DOPC-based liposomes ($DOPC_{PS\text{-}CAT}$) and DMPC-

**Table 1.** Light-driven $CO_2$ reduction (405 nm LED, headspace GC sampling), $TON_{CO}$ and selectivity results respectively. Liposomes samples, with a composition of 100:1:0.5 of (main lipid):(14:0 PEG2000 PE):**PS-CAT** with c(main lipid) = 0.3 mM and c(sodium ascorbate) = 0.1 M: (Entries 1–3) maximum performance within 56 h irradiation. (Entries 4–6) after 24 h of irradiation. (Entries 7–9) performance with c(main lipid) = 0.03 mM after 24 h of irradiation. (Entries 10,11) control experiments after 24 h of irradiation. Light-active organic mixtures of **PS-CAT** and 1,3-dimethyl-2-phenylbenzimidazoline (BIH) as sacrificial electron donor and proton source in N-Methyl-2-pyrrolidone (NMP) as solvent, with and without water presence: (Entries 12 and 13) after 24 h of irradiation. (Entries 14–17) reported liposome-based systems.

| Entry | Host Lipid | Solvent | Sacrificial Electron Donor (SED) | C (Lipid) [μM] | c(CAT) [μM] | CO (nmol) | $TON_{CO}$ | Selectivity (%) | Comment | Refs. |
|---|---|---|---|---|---|---|---|---|---|---|
| 1 | DPPC | Water | Ascorbate | 300 | 1.5 | 1012 ± 131 | 338 ± 44 | >99[a] | 56 h | |
| 2 | DOPC | Water | Ascorbate | 300 | 1.5 | 695 ± 157 | 232 ± 52 | >99[a] | 56 h | |
| 3 | DMPC | Water | Ascorbate | 300 | 1.5 | 358 ± 67 | 119 ± 22 | >99[a] | 56 h | |
| 4 | DPPC | Water | Ascorbate | 300 | 1.5 | 395 ± 101 | 132 ± 34 | >99[a] | 24 h | |
| 5 | DOPC | Water | Ascorbate | 300 | 1.5 | 625 ± 124 | 209 ± 41 | >99[a] | 24 h | |
| 6 | DMPC | Water | Ascorbate | 300 | 1.5 | 358 ± 67 | 119 ± 22 | >99[a] | 24 h | |
| 7 | DPPC | Water | Ascorbate | 30 | 1.5 | 292 ± 21 | 97 ± 14 | >99[a] | 24 h | |
| 8 | DOPC | Water | Ascorbate | 30 | 1.5 | 281 ± 42 | 94 ± 16 | >99[a] | 24 h | |
| 9 | DMPC | Water | Ascorbate | 30 | 1.5 | 195 ± 55 | 64 ± 12 | >99[a] | 24 h | |
| 10 | DPPC | Water | Ascorbate | 300 | 1.5 | 33 ± 5 | 11 ± 2 | >99[a] | No $CO_2$ bubbling | |
| 11 | DPPC | Water | – | 300 | 1.5 | 18 ± 5 | 6 ± 2 | >99[a] | No $CO_2$ bubbling | |
| 12 | – | NMP | BIH | – | 10 | 171 | 17 | 76 | | |
| 13 | – | NMP-water | BIH | – | 10 | 347 ± 48 | 35 ± 5 | >99[a] | | |
| 14 | DPPC | Water | Ascorbate | 600 | 2.5 | 109 ± 8 | 14 ± 1 | 98 ± 1 | Lower TON [Ru]-PS, [Re]-CAT | [11] |
| 15 | DMPC | Water | Ascorbate | 100 | 0.02 | 44 ± 5 | 735 ± 91 | 78 ± 4 | Lower selectivity, [Ru]-PS, [Co]-CAT | [2] |
| 16 | DPPC | Water | Ascorbate | 120 | 14 | 2100 | 50 | 94 | [Ir]-PS, [Re]-CAT | [33] |
| 17 | DPPC | Water | Ascorbate | 0.12 | 40 | 6200 | 190 | 98 | [Ru]-PS, [Re]-CAT | [36] |

[a] $H_2$ and $CH_4$ amounts were not detected above the detection limit (0.05 nmol $L^{-1}$).

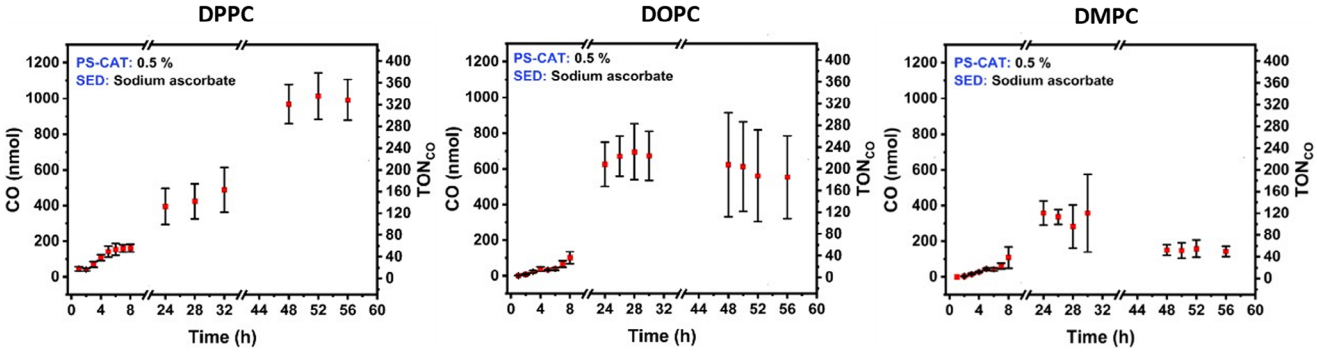


**Figure 3.** Time-dependent $CO_2$ reduction activity and $TON_{CO}$ results of the light-active DPPC, DOPC, and DMPC vesicles, under irradiation of 405 nm LED and monitored over 56 h. Experimental conditions: liposomes sample in $CO_2$ atmosphere with a composition of 100:1:0.5 of main lipid:(14:0 PEG2000 PE):PS-CAT, with c(main lipid) = 0.3 mM, c(PS-CAT) = 1.5 μM, and c(sodium ascorbate) = 0.1 M. All values were acquired in triplicate with error bars presenting the standard deviation.

based liposomes ($DMPC_{PS\text{-}CAT}$) produced approximately 2 to 4 times less CO ($TON_{CO,DOPC}$ = 184 ± 78, $TON_{CO,DMPC}$ = 47 ± 10) than $DPPC_{PS\text{-}CAT}$ after 56 h of irradiation (Figure 3). In addition, $DPPC_{PS\text{-}CAT}$ showed a superior activity already in the first 4 h of the reaction, characterized by $TOF_{CO,DPPC}$ = 6.8, $TOF_{CO,DOPC}$ = 3.8, and $TOF_{CO,DMPC}$ = 3.1 $h^{-1}$ (first 4 h). The early stages of the reaction were chosen for the determination of TOF, as this time frame is less affected by catalyst decomposition and decreasing quencher concentration.[31] In terms of catalysis performance, $DPPC_{PS\text{-}CAT}$ proved to have the most stable catalysis performance over time, indicated by the CO production leveling off after 52 h of irradiation (Figure 3). In contrast, $DOPC_{PS\text{-}CAT}$ and $DMPC_{PS\text{-}CAT}$ reached steady points of CO production and started to lose their activity after 24 h of irradiation. In the case of $DMPC_{PS\text{-}CAT}$, a decrease was observed after 30 h. This decrease might be due to some leakage. No follow-up $CO_2$-reduction products such as $CH_4$ or $C_2H_4$ or $C_2H_6$, were detected as mentioned above and shown in Figures S4, S5, S9, and S10.

**Table 2.** Summary of Stern–Volmer constants, quenching rate constants, and lifetime from mechanistic studies. Experimental conditions: DPPC, DMPC, and DOPC liposomes samples at 5 mM of main lipid, with a composition of 100:1:0.5 of (main lipid):(14:0 PEG2000 PE):**PS-CAT**, prepared in 0.1 M sodium hydrogencarbonate solution containing sodium ascorbate as sacrificial electron donor. Values are reported as mean values ± standard deviation.

| Liposome | $\tau_0$ (ps) | $K_{sv}$ (L mol$^{-1}$) | $k_q$ (L mol$^{-1}$ s$^{-1}$) |
|---|---|---|---|
| $DPPC_{PS\text{-}CAT}$ | 481 | 3.5 ± 0.5 | (7.0 ± 2.0)·10$^9$ |
| $DOPC_{PS\text{-}CAT}$ | 475 | 1.2 ± 0.5 | (2.5 ± 1.3)·10$^9$ |
| $DMPC_{PS\text{-}CAT}$ | 443 | 1.1 ± 0.2 | (2.5 ± 0.7)·10$^9$ |

Considering the structural stability, the average vesicle size, indicated by $Z_{Avg}$ from DLS, of $DMPC_{PS\text{-}CAT}$ had decreased after 56 h of irradiation (129 ± 9 to 103 ± 11 nm), whereas the $Z_{Avg}$ of $DPPC_{PS\text{-}CAT}$ showed no significant difference (170 ± 7 to 176 ± 9 nm) and the $Z_{Avg}$ of $DOPC_{PS\text{-}CAT}$ had slightly increased (133 ± 12 to 165 ± 13 nm) comparing the vesicle sizes before and after the irradiation. These results indicate that $DPPC_{PS\text{-}CAT}$ liposomes are structurally more stable than the more fluid liposomes tested here which might support the high activity in light-driven catalysis. Additionally, the TONs and TOFs were determined based on the amounts of **PS-CAT** added during sample preparation but this amount might vary and influence the calculation of the performance indicators, depending on the lipid bilayer specific uptake.[10,11]

The effect of the local concentration of **PS-CAT** within the lipid bilayer was characterized at low vs high **PS-CAT** loading within the membrane. In addition to the already discussed experiments at 100:1:0.5 molar ratio of the (main lipid):(14:0 PEG2000 PE):**PS-CAT** at overall concentrations of $c_{main\ lipid}$ = 0.3 mM, $c_{PS\text{-}CAT}$ = 1.5 μM, the composition 100:10:5 was tested at overall concentrations of $c_{main\ lipid}$ = 0.03 mM, $c_{PS\text{-}CAT}$ = 1.5 μM. At higher loading and identical catalyst concentration, we obtained $TON_{CO,DPPC} = 97 \pm 14$, $TON_{CO,DOPC} = 94 \pm 16$, and $TON_{CO,DMPC} = 65 \pm 12$ after 24 h of irradiation, which corresponds to approximately 20% to 50% less CO than in the case of liposomes with normal **PS-CAT** loading ($TON_{CO,DPPC} = 132 \pm 34$, $TON_{CO,DOPC} = 209 \pm 41$, and $TON_{CO,DMPC} = 119 \pm 22$). This trend might be caused by bimolecular catalyst deactivation[24] or bimolecular quenching of the excited state of the PS in **PS-CAT** which can inhibit productive electron transfer (ET) pathways between PS and CAT or PS and SED.[2,42] Indeed, the confocal imaging (Figure 2B) suggests some degree of aggregation of **PS-CAT** in $DPPC_{PS\text{-}CAT}$ even in a lower **PS-CAT** concentration. Therefore, avoiding the high local concentration of **PS-CAT** in the lipid bilayer can improve the catalytic performance in $CO_2$RR. A summary of different photocatalytic conditions to obtain the highest $TON_{CO}$ and selectivity >99%, using **PS-CAT** in $CO_2$RR are depicted (Figure 4 and Table 1).

### 2.3. Excited-State Electron-Transfer Dynamics

A previous study on light-driven $H_2$ evolution with **PS-CAT** in a homogeneous solution has shown that the photocatalytic reduction cycle starts with the light-driven reduction of the CAT moiety by the PS moiety.[31] However, the situation in lipid bilayers might be different, and we investigated initial electron transfer between the excited state **PS-CAT** and the terminal electron donor ascorbate in a Stern–Volmer assay via time-resolved and steady-state luminescence spectroscopy. The Stern–Volmer equation (Equation 4) was applied to obtain quencher concentration [Q], the quenching ($k_q$) and Stern–Volmer ($K_{SV}$) constants. The fluorescence intensity I ($I_0$) and concentration of sodium ascorbate [Q] data are provided in the Supporting Information.

$$\frac{I_0}{I} = 1 + K_{SV}[Q] = 1 + k_q \tau_0 [Q] \quad (4)$$

Experimentally, the excited-state lifetime $\tau_0$ was between 440 and 480 ps in all lipid environments (Table 2). In the presence of ascorbate as an electron donor, the lifetimes of the liposomes remained almost unchanged irrespective of the quencher concentration. However, the emission intensity decreased in all cases with increasing quencher concentration (Supporting Information) which leads to the conclusion that fluorescence quenching occurs via a static quenching mechanism in all types of liposomes. Static quenching takes place when the quencher, that is, ascorbate, is pre-associated to the PS prior to photoexcitation, indicating that ascorbate anions are assembled at the membrane surface of all investigated liposomes. The quenching in $DPPC_{PS\text{-}CAT}$ is by approximately factor 3 more effective than the two other lipid matrices following the series: $DPPC_{PS\text{-}CAT} > DOPC_{PS\text{-}CAT} \approx DMPC_{PS\text{-}CAT}$, aligning with the relative results on photocatalytic performance indicators TOF and TON in all three liposomes.

To gain further insight into the static quenching between **PS-CAT** and ascorbate, the zeta-potential was measured in presence and absence of sodium ascorbate. The zeta potential $\zeta$ relates to the surface charge, thus providing insights into ascorbate assembly at the membrane surface. In the absence of sodium ascorbate, the zeta potential was slightly negative in all cases: $\zeta(DPPC_{PS\text{-}CAT}) = -0.194$ mV, $\zeta(DOPC_{PS\text{-}CAT}) = -0.205$ mV, and $\zeta(DMPC_{PS\text{-}CAT}) = -0.115$ mV, due to the negatively charged 14:0 PEG2000 PE lipid (Table S3).[43–45] In the presence of sodium ascorbate, the zeta potential of all liposomes becomes significantly more negative with $\zeta(DPPC_{PS\text{-}CAT}) = -1.581$ mV, $\zeta(DOPC_{PS\text{-}CAT}) = -0.406$ mV, and $\zeta(DMPC_{PS\text{-}CAT}) = -0.326$ mV (Table S3). It is reasonable to assume that negatively charged species–likely ascorbate–assemble at the lipid bilayer-water interface upon ascorbate addition.[46] These zeta potential results support the findings from the Stern–Volmer-quenching dynamics and association of ascorbate ions to the liposome surface, close to the **PS-CAT** molecules. Furthermore, the data suggest that more ascorbate is assembled at the $DPPC_{PS\text{-}CAT}$ surface, which has the lowest diffusion mobility, compared to the $DOPC_{PS\text{-}CAT}$ and $DMPC_{PS\text{-}CAT}$ surface, this is a trend that is also observed with the Stern–Volmer-quenching dynamics.

To summarize the results of the fluorescence quenching and zeta potential measurements, the Stern–Volmer quenching dynamics can be explained by static quenching with ascor-

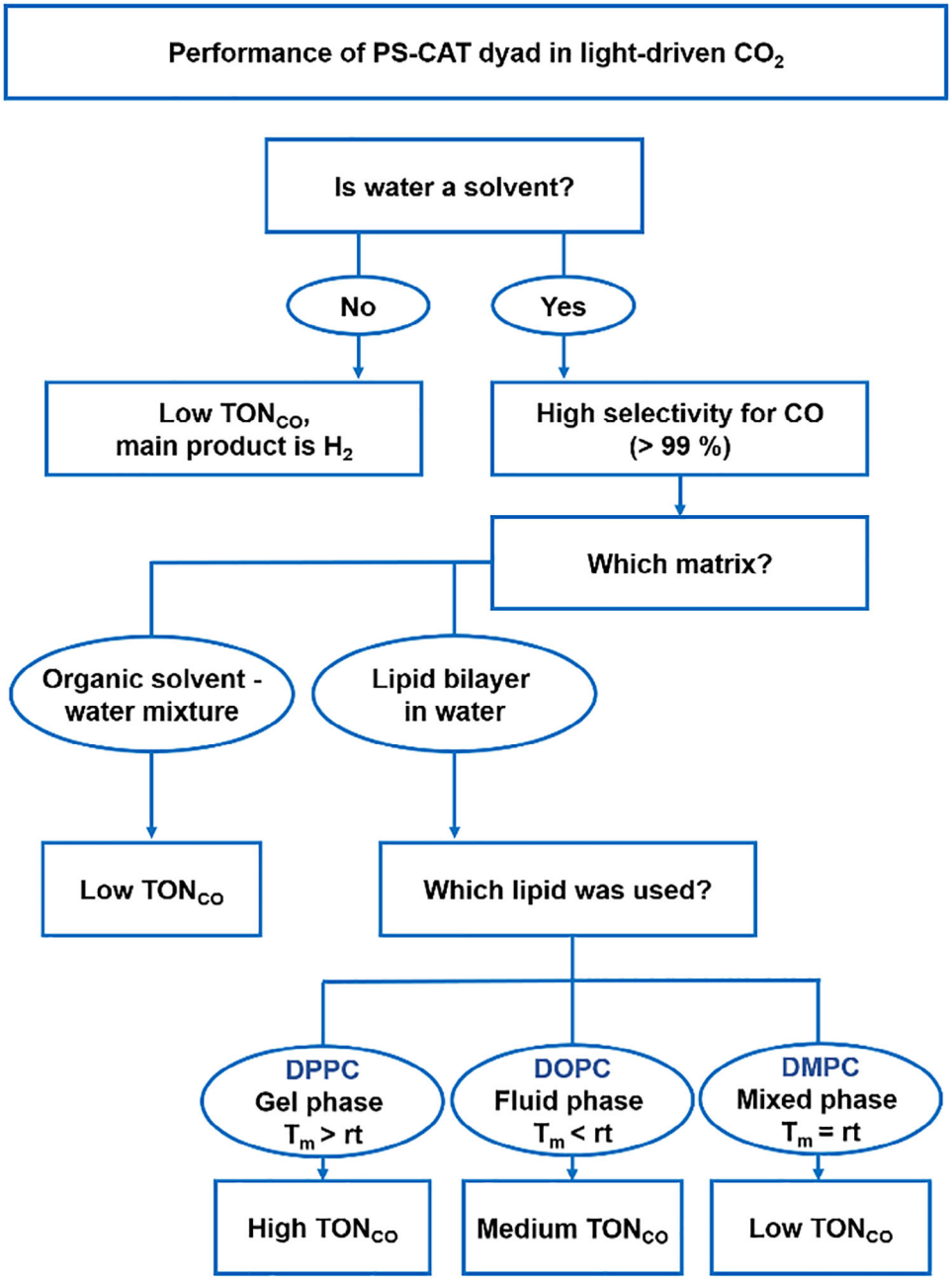


**Figure 4.** Decision tree depicting the best photocatalytic conditions for PS-CAT to obtain high CO selectivity (>99%) and superior $TON_{CO}$ within lipid bilayer, in comparison to the corresponding homogeneous system in absence and presence of water.

bate anions assembled on the membrane surface. Moreover, the Stern–Volmer constant and zeta potential exhibited a similar trend for phospholipids, with $DPPC_{PS\text{-}CAT}$ exhibiting the largest absolute value of both $k_q$ and $\zeta$, followed by $DOPC_{PS\text{-}CAT}$ and $DMPC_{PS\text{-}CAT}$. The quenching dynamics are also in good agreement with the catalytic activity, which is strongly increased by electron transfer from the electron donor to the photoexcited **PS-CAT**, a key factor in $CO_2$RR with our dyad-liposome integrated system. This result is in line with another study on photocatalytic $H_2$ evolution with a [Ru]-PS and [Mo]-CAT in lipid bilayers, where we found as well that initial quenching determines light-driven catalysis performance.[3]

## 3. Conclusions

In summary, biomimetic phospholipid bilayers were integrated with a [FeFe]-hydrogenase mimic **PS-CAT**, and the resulting unilamellar stable liposome structures enable light-driven $CO_2$ reduction in water. Initially, the CO selectivity against $H_2$ production in photocatalytic processes was investigated using $DPPC_{PS\text{-}CAT}$, revealing a CO selectivity of >99%. We found that this high CO selectivity was due to the presence of water as confirmed by experiments with a **PS-CAT** in organic solvents with and without the presence of water. Subsequently, comparative experiments for photocatalytic $CO_2$RRs were performed

with different lipid samples, that is, $DPPC_{PS\text{-}CAT}$, $DOPC_{PS\text{-}CAT}$, and $DMPC_{PS\text{-}CAT}$. Thereby, $DPPC_{PS\text{-}CAT}$ exhibited the highest $TON_{CO}$ (338 ± 44, 52 h) and $TOF_{CO}$ (6.8 $h^{-1}$), indicating that the gel-phase DPPC liposomes provide superior photocatalytic stability and efficiency. Furthermore, static quenching of **PS-CAT** emission was observed by emission quenching experiments in the presence of ascorbate. The zeta potential results indicated this static quenching proceeded with the assembly of **PS-CAT** and the electron donor ascorbate at the membrane-water interface. It was also observed that the emission quenching rate by the SED was most efficient in DPPC lipid bilayers, which have the lowest diffusion mobility. The superior quenching rate may explain the stronger catalytic performance of $DPPC_{PS\text{-}CAT}$. However, further mechanistic investigations are needed to elucidate the details of light-driven $CO_2$ reduction by [FeFe]-hydrogenase mimics in the presence of water.

## Acknowledgements

The authors gratefully acknowledge the Deutsche Forschungsgemeinschaft (DFG, project TRR234 "CataLight" project number 364549901, projects C5, B10, and B8) for financial support. Andrea Pannwitz gratefully acknowledges financial support by the Vector Stiftung (project number P2019-0110) as well as the CZS-Stiftung. Chizuru Kasahara and Stefanie Gräfe highly acknowledge funding from the Carl Zeiss Foundation, via the "Perspectives" project "Vitrimers". Part of this research has also been financially supported by the Research Unit DeKarbon–*Selective Deposition and Chemical Conversion of Carbon Dioxide on Nanostructured Polymer Materials* (FTI Thüringen PERSONEN, 2022 FGR 0001), supported by the Free State of Thuringia and the European Social Fund Plus. The authors thank Dr. P. Saini Urhan for supervising $^{13}C$-labelling experiments and GC-MS measurements, and Ms. V. T. Sundarraj for supervising DLS measurements. The NMR platform at Jena University carried out all NMR spectroscopy measurements, and the authors thank Dr. D. Diaz for consulting on detecting $CO_2RR$ products by NMR. Acquisition of the 500 MHz NMR spectrometer was supported by a grant "Forschungsgroßgeräte nach Art. 91b", grant INST 275/442–1 FUGG of the Deutsche Forschungsgemeinschaft (DFG). We thank N. Sinambela for the scientific discussion. The confocal images were recorded at the Core Facility for Confocal and Multiphoton Microscopy at Ulm University which is supported by the DFG through project number 91BGG INST 381/39–1. We thank Dr. Christian Bökel for his support during confocal microscopy. Some figures were created with Biorender.com.

Open access funding enabled and organized by Projekt DEAL.

## Conflict of Interests

The authors declare no conflict of interest.

## Data Availability Statement

The data that support the findings of this study are available in the supplementary material of this article.

**Keywords:** [FeFe]-Hydrogenase mimics · $CO_2$ reduction · Photocatalysis · Selectivity

[1] M. Hansen, S. Troppmann, B. König, *Chem. - Eur. J.* **2016**, *22*, 58–72.
[2] S. Rodríguez-Jiménez, H. Song, E. Lam, D. Wright, A. Pannwitz, S. A. Bonke, J. J. Baumberg, S. Bonnet, L. Hammarström, E. Reisner, *J. Am. Chem. Soc.* **2022**, *144*, 9399–9412.
[3] A. Abbas, E. Oswald, J. Romer, A. Lenzer, M. Heiland, C. Streb, C. Kranz, A. Pannwitz, *Chem. Eur. J.* **2023**, *29*, e202302284.
[4] B. Limburg, E. Bouwman, S. Bonnet, *ACS Catal.* **2016**, *6*, 5273–5284.
[5] B. Limburg, J. Wermink, S. S. Van Nielen, R. Kortlever, M. T. M. Koper, E. Bouwman, S. Bonnet, *ACS Catal.* **2016**, *6*, 5968–5977.
[6] M. Petersen, R. E. P. Nau, A. Pannwitz, T. Wilke, *CHEMKON* **2023**, *30*, 260–266.
[7] S. Troppmann, B. König, *Chem. Eur. J.* **2014**, *20*, 14570–14574.
[8] H. Hu, Z. Wang, L. Cao, L. Zeng, C. Zhang, W. Lin, C. Wang, *Nat. Chem.* **2021**, *13*, 358–366.
[9] A. Pannwitz, D. M. Klein, S. Rodríguez-Jiménez, C. Casadevall, H. Song, E. Reisner, L. Hammarström, S. Bonnet, *Chem. Soc. Rev.* **2021**, *50*, 4833–4855.
[10] N. Sinambela, J. Bösking, A. Abbas, A. Pannwitz, *ChemBioChem* **2021**, *22*, 3140–3147.
[11] D. M. Klein, S. Rodríguez-Jiménez, M. E. Hoefnagel, A. Pannwitz, A. Prabhakaran, M. A. Siegler, T. E. Keyes, E. Reisner, A. M. Brouwer, S. Bonnet, *Chem. Eur. J.* **2021**, *27*, 17203–17212.
[12] W. T. Eckenhoff, R. Eisenberg, *Dalton Trans.* **2012**, *41*, 13004.
[13] A. D. Handoko, K. Li, J. Tang, *Curr. Opin. Chem. Eng.* **2013**, *2*, 200–206.
[14] L. Z. Wu, B. Chen, Z. J. Li, C. H. Tung, *Acc. Chem. Res.* **2014**, *47*, 2177–2185.
[15] F. Wang, *ChemSusChem* **2017**, *10*, 4393–4402.
[16] H.-L. Wu, X.-B. Li, C.-H. Tung, L.-Z. Wu, *Chem. Commun.* **2020**, *56*, 15496–15512.
[17] S. Yoshino, T. Takayama, Y. Yamaguchi, A. Iwase, A. Kudo, *Acc. Chem. Res.* **2022**, *55*, 966–977.
[18] G. Liao, G. Ding, B. Yang, C. Li, *Precis. Chem.* **2024**, *2*, 49–56.
[19] N.-N. Vu, S. Kaliaguine, T.-O. Do, *Adv. Funct. Mater.* **2019**, *29*, 1901825.
[20] E. Karamian, S. Sharifnia, *J. $CO_2$ Util.* **2016**, *16*, 194–203.
[21] M. F. Kuehnel, K. L. Orchard, K. E. Dalle, E. Reisner, *J. Am. Chem. Soc.* **2017**, *139*, 7217–7223.
[22] K. Holá, M. V. Pavliuk, B. Németh, P. Huang, L. Zdražil, H. Land, G. Berggren, H. Tian, *ACS Catal.* **2020**, *10*, 9943–9952.
[23] K. E. Dalle, J. Warnan, J. J. Leung, B. Reuillard, I. S. Karmel, E. Reisner, *Chem. Rev.* **2019**, *119*, 2752–2875.
[24] J. Amaro-Gahete, M. V. Pavliuk, H. Tian, D. Esquivel, F. J. Romero-Salguero, S. Ott, *Coord. Chem. Rev.* **2021**, *448*, 214172.
[25] P. Ceccaldi, K. Schuchmann, V. Müller, S. J. Elliott, *Energy Environ. Sci.* **2017**, *10*, 503–508.
[26] M. Cheng, Y. Yu, X. Zhou, Y. Luo, M. Wang, *ACS Catal.* **2019**, *9*, 768–774.
[27] M. Cheng, X. Zhang, Y. Zhu, M. Wang, *Chin. J. Catal.* **2021**, *42*, 310–319.
[28] C. D. Windle, R. N. Perutz, *Coord. Chem. Rev.* **2012**, *256*, 2562–2570.
[29] S. Morra, *Front. Microbiol.* **2022**, *13*, 853626.
[30] P. Buday, C. Kasahara, E. Hofmeister, D. Kowalczyk, M. K. Farh, S. Riediger, M. Schulz, M. Wächtler, S. Furukawa, M. Saito, D. Ziegenbalg, S. Gräfe, P. Bäuerle, S. Kupfer, B. Dietzek-Ivanšić, W. Weigand, *Angew. Chem. Int. Ed Engl.* **2022**, *61*, e202202079.
[31] C. Kasahara, K. Rediger, M. Micheel, P. Liebing, S. Gräfe, S. Kupfer, M. Wächtler, W. Weigand, *ChemCatChem* **2024**, *16*, e202400247.
[32] R. Becker, T. Bouwens, E. C. F. Schippers, T. van Gelderen, M. Hilbers, S. Woutersen, J. N. H. Reek, *Chem. Eur. J.* **2019**, *25*, 13921–13929.
[33] S. Takizawa, T. Okuyama, S. Yamazaki, K. Sato, H. Masai, T. Iwai, S. Murata, J. Terao, *J. Am. Chem. Soc.* **2023**, *145*, 15049–15053.
[34] I. M. Le-Deygen, A. S. Safronova, I. M. Kolmogorov, *Russ. J. Bioorg. Chem.* **2022**, *48*, 710–719.

[35] D. Kowalczyk, P. Li, A. Abbas, J. Eichhorn, P. Buday, M. Heiland, A. Pannwitz, F. H. Schacher, W. Weigand, C. Streb, D. Ziegenbalg, *ChemPhotoChem* **2022**, *6*, e202200044.
[36] N. Ikuta, S.-Y. Takizawa, S. Murata, *Photochem. Photobiol. Sci.* **2014**, *13*, 691–702.
[37] Y. Xiao, H. T. Zhang, M. T. Zhang, *J. Am. Chem. Soc.* **2024**, *146*, 28832–28844.
[38] F. Droghetti, F. Lemken, L. Rulíšek, A. Ruggi, M. Natali, *ACS Catal.* **2024**, *14*, 16920–16935.
[39] W. Xie, J. Xu, U. Md Idros, J. Katsuhira, M. Fuki, M. Hayashi, M. Yamanaka, Y. Kobori, R. Matsubara, *Nat. Chem.* **2023**, *15*, 794–802.
[40] S. Troppmann, B. König, *ChemistrySelect* **2016**, *1*, 1405–1409.
[41] S. Troppmann, E. Brandes, H. Motschmann, F. Li, M. Wang, L. Sun, B. König, *Eur. J. Inorg. Chem.* **2016**, 554–560.
[42] H. Song, A. Amati, A. Pannwitz, S. Bonnet, L. Hammarström, *J. Am. Chem. Soc.* **2022**, *144*, 19353–19364.
[43] W. Kong, Y. Wei, Z. Dong, W. Liu, J. Zhao, Y. Huang, J. Yang, W. Wu, H. He, J. Qi, *J. Nanobiotechnol.* **2024**, *22*, 553.
[44] K. Chen, A. Najer, P. Charchar, C. Saunders, C. Thanapongpibul, A. Klöckner, M. Chami, D. J. Peeler, I. Silva, L. Panariello, K. Karu, C. N. Loynachan, L. C. Frenette, M. Potter, J. S. Tregoning, I. P. Parkin, A. M. Edwards, T. B. Clarke, I. Yarovsky, M. M. Stevens, *Nat. Commun.* **2024**, *15*, 10321.
[45] R. Tenchov, J. M. Sasso, Q. A. Zhou, *Bioconjugate Chem.* **2023**, *34*, 941–960.
[46] M. Łukawski, P. Dałek, W. Witkiewicz, M. Przybyło, M. Langner, *Chem. Phys. Lipids* **2020**, *232*, 104950.

Manuscript received: April 17, 2025
Accepted manuscript online: April 24, 2025
Version of record online: April 29, 2025